Diamond & Related Materials 64 (2016) 169–176

Contents lists available at ScienceDirect

Diamond & Related Materials

journal homepage: www.elsevier.com/locate/diamond

Application of thin diamond films in low-coherence fiber-optic Fabry Pérot displacement sensor

D. Milewska [1], K. Karpienko [1], M. Jędrzejewska-Szczerska *

Gdańsk University of Technology, Department of Electronics, Telecommunication and Informatics, 11/12 Narutowicza, 80-233 Gdansk, Poland

ARTICLE INFO

Article history:
Received 22 December 2015
Received in revised form 12 February 2016
Accepted 18 February 2016
Available online 21 February 2016

Keywords:
Fiber-optic sensor
Fabry–Pérot interferometer
Displacement sensors
Diamond

ABSTRACT

The novel fiber-optic low coherence sensor with thin diamond films is demonstrated. The undoped and boron-doped diamond films were elaborated by the use of the microwave plasma enhanced chemical vapor deposition (μPE CVD) system. The optical signal from the Fabry–Pérot cavity made with the application of those thin films is sensitive to displacement. The sensor characterization was made in the range of 0–600 μm. The measurements were performed using two superluminescent diodes (SLD) with central wavelengths of 1290 mm and 1550 mm and the output signal was analyzed by the measurement of the modulation change of spectral pattern. Furthermore, very good coefficient of the determination $R^2 > 0.9565$ and the visibility of optical measured signal equal to 95.6% were achieved.

1. Introduction

Fiber optic interferometric sensors are dedicated to measure the broad range of physical and biochemical quantities, such as temperature, and refractive index [1–5]. However, the displacement sensor gives us the opportunity to measure many quantities, whose changes can be transferred into the displacement change for example: pressure, velocity, acceleration and others [6–9].The application of low-coherence interferometry in fiber-optic sensor gives us the possibility to obtain very high value of resolution and dynamic of measurement as in the conventional interferometry [10–12]. However, by the use of low-coherence interferometry, it is possible to obtain sensors, what is the proof for any changes of the optical signal intensity of the measured signal. It is so because in low-coherence sensor the information is encoded in the changes of the spectrum of measured signal. Fiber-optic interferometric sensors can be done in many configurations, however, the application of the low-finesse Fabry–Pérot interferometer in reflective mode was chosen due to the broad range of its good points, including inter alia: relatively simple configuration, potentially low cost, high resolution and low thermal inertia. Furthermore, due to its small size, it is possible to make nearly point wise temperature measurement. Recently, optical fiber sensors, which make the optic sensors more appealing than ever, are to be obtained in a simple and inexpensive manner [13–15]. Furthermore, the metrological parameters of such sensors are determined by the materials which were used for the construction of their elements such as mirrors. Most commonly used, as a reflective surface in the Fabry–Pérot interferometers, are silver mirrors. This material is cheap and sufficiently well reflecting a light beam, however, it is chemically unstable and sensitive to mechanical damage. Hence, the need to implement other materials, such as the reflective surfaces in order to achieve greater resistance to harmful mechanical and chemical conditions, seems to be of the great range.

In spite of this, in the last years diamond has started to be an attractive topic in engineers' applications. Different applications of diamond films have been reported so far, e.g., microelectromechanical systems (MEMS), high power electronics, high-frequency devices, electrochemical sensors or protective coatings for biomedical applications [16].

Thin diamond films are mainly synthesized using microwave plasma enhanced chemical vapor deposition (μPE CVD). This technique allows the manufacture of diamond thin films representing such structural properties as: thickness, grain size, texture, chemical composition, defect concentration and surface morphology. The abovementioned features are adjusted by changing the process conditions including temperature, thickness or doping, along with the selection of the substrate material and, moreover, have a strong impact on fundamental properties that involve optical, mechanical, electrical and other attributes of diamond films [17–20].

Here, the fiber-optic displacement sensor with new reflective layer made of silicon protected with thin diamond film is described. The undoped diamond and boron-doped diamond films were deposited on silicon substrate by the use of microwave plasma enhanced chemical vapor deposition. In the presented displacement sensor, thin diamond films have been used due to their outstanding properties such as: biocompatibility, great chemical stability, remarkable hardness, high

* Corresponding author.
E-mail address: mjedrzej@eti.pg.gda.pl (M. Jędrzejewska-Szczerska).
[1] Equally contributing authors.

http://dx.doi.org/10.1016/j.diamond.2016.02.015

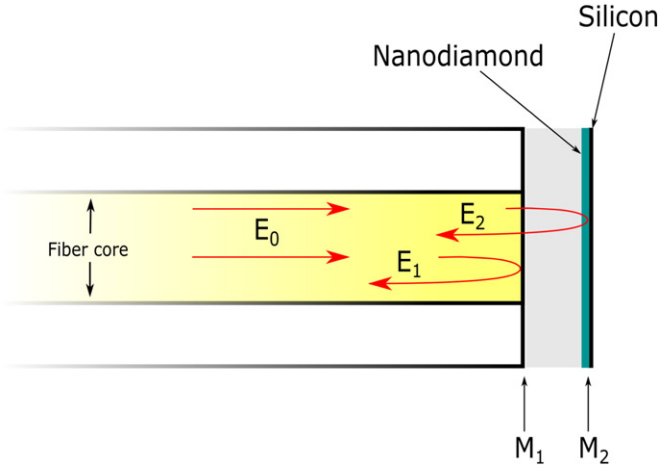

Fig. 1. Extrinsic Fabry–Pérot interferometer working in reflective mode: M_1, M_2 — cavity mirrors, E_0 — the amplitude of an electric vector of an incident wave; E_1, E_2 — the amplitude of an electric vector of wave reflected of the first and second mirrors, respectively.

thermal conductivity, optical transparency. The sensor's optimal construction was thoroughly examined so that the best metrological parameters can be reached.

2. Theory

The developed sensor was designed as an extrinsic Fabry–Pérot working in the reflective mode, as shown in Fig. 1. The cavity mirrors M_1 and M_2 use Fresnel reflection at the boundary between the single mode optical fiber and the surrounding medium, as well as, the surrounding medium and diamond films.

The theory of Fabry–Pérot interferometer has been discussed in the literature [13–14,21], though without any very important effects. The analysis of the work of the fiber-optic extrinsic Fabry–Pérot interferometer should take into consideration: power loss effect in Fabry–Pérot cavity caused by light beam divergence, the fact that the coefficient reflection of the mirror differentiates from each other and also the multi-beam interference in Fabry–Pérot cavity. All of those problems affect the work of the fiber-optic Fabry–Pérot interferometer and, therefore, they are discussed in this section. The Fabry–Pérot cavity is formed by two parallel mirrors with reflectivity R_1 and R_2. Amplitudes of waves reflected from mirrors in multi-beam interference with Gaussian beam expansion-induced power attenuation can be expressed as [13–14,21]:

$$\begin{aligned} E_1 &= -\sqrt{R_1}\ E_0 \\ E_2 &= \sqrt{R_2}(1-R_1)\ E_0\sqrt{\alpha(x)} \\ E_3 &= R_2\sqrt{R_1}(1-R_1)\ E_0\left(\sqrt{\alpha(x)}\right)^2 = E_2\ \sqrt{R_1R_2}\sqrt{\alpha(x)} \\ &\cdots\cdots\cdots\cdots \\ E_{N+1} &= E_N\ \sqrt{R_1R_2}\sqrt{\alpha(x)} \qquad for \qquad N\geq 2 \end{aligned} \tag{1}$$

where: E_0 — the amplitude of an electric vector of an incident wave; E_1 — the amplitude of an electric vector of i-incident wave; R_1, R_2 — reflectivity of the first and the second mirror of the interferometer respectively; $\alpha(x)$ — the attenuation coefficient of optical intensity of a light beam in the Fabry–Pérot cavity; x — length of the Fabry–Pérot cavity.

The resultant reflected scalar E_r wave is given by:

$$E_r = E_1 + E_2 + E_3 + \cdots\cdots\cdots\cdots \tag{2}$$

and when changes the phase of the interfering beam is taken into consideration:

$$E_r = E_1 e^{i\delta} + E_2 e^{-i2\delta} + \cdots\cdots + E_n e^{-i2N\delta} \tag{2.a}$$

where: δ — phase difference: $\delta = 4\pi \frac{nx}{\lambda}$, x — length of the Fabry–Pérot cavity.

Hence, it is possible to get the reflected intensity:

$$I_r = \langle E_r E_r^* \rangle \tag{3}$$

where: the brackets $\langle\rangle$ — denote time averages; the asterisk * — the complex conjugation.

It is known that when the value of reflectivity of interferometer mirrors (R_1, R_2) is small and cavity length x: $x \gg \lambda$, then the transfer function of such interferometer is essentially of a two-beam interferometer [14]. Taking this into account, amplitudes E_{1r} and E_{2r} of waves reflected from the first and the second surface can be written as:

$$\left.\begin{aligned} E_{1r} &= -\sqrt{R_1}\cdot E_0 \\ E_{2r} &= (1-R_1)\sqrt{\alpha(x)R_2}\cdot E_0 \end{aligned}\right\}. \tag{4}$$

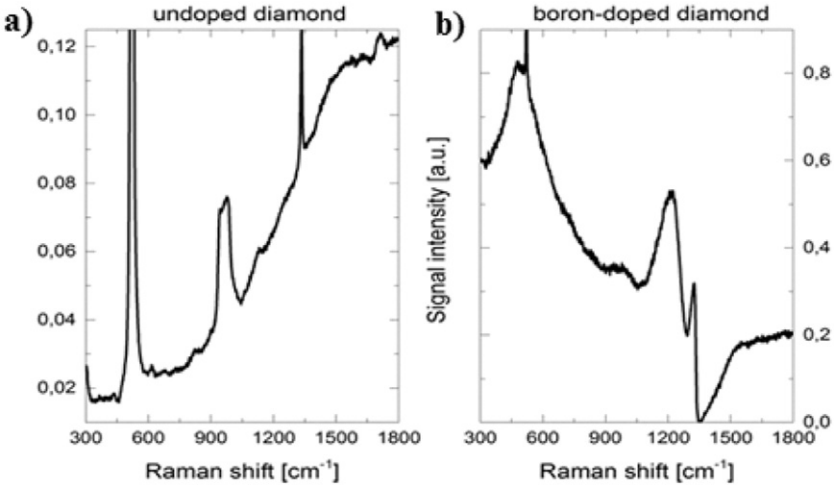

Fig. 2. Raman spectra of diamond thin films: a) undoped diamond, b) boron-doped diamond.

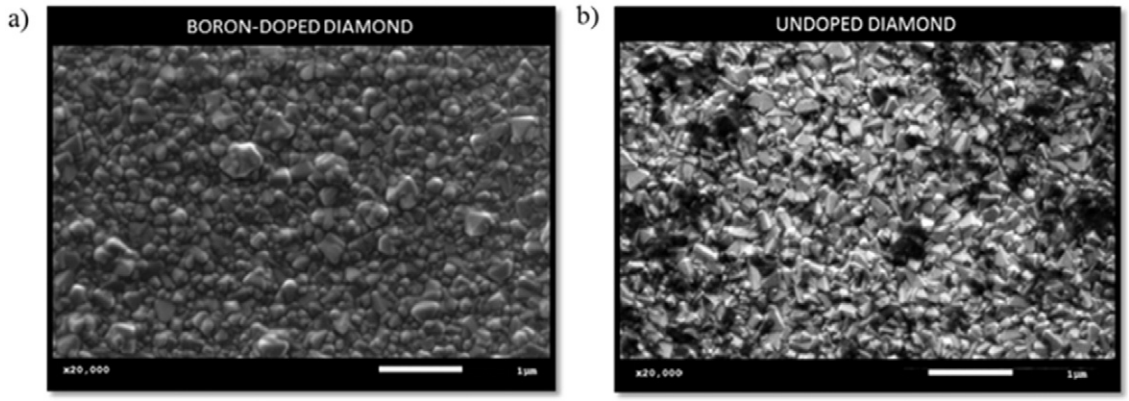

Fig. 3. SEM images of diamond films deposited on silicon substrate: a) boron-doped diamond, b) undoped diamond.

The optical intensity at the output of such interferometer can be expressed by Eq. (5) as follows:

$$I_r = I_c[1 + V_0 \cdot \cos\delta] \tag{5}$$

where: V_0 — the visibility of interference fringes, I_c — the static component of the optical signal expressed by:

$$I_c = I_0\left[R_1 + (1-R_1)^2 \cdot R_2\alpha(x)\right] \tag{6}$$

$I_0 = E_0^2$ — the intensity of light incident on the first boundary surface of the interferometer.

In this situation V_0 visibility of the interference pattern (V_0) in the spectral domain is expressed [15]:

$$V_0 = \frac{2\sqrt{\alpha(x)R_1R_2}(1-R_1)}{R_1 + (1-R_1)^2\alpha(x)R_2}. \tag{7}$$

In order to attain the best metrological parameters of the interferometer, the value of the visibility of the measured signal V_0 should get maximum what helps to decrease the required signal to noise ratio of the detection set-up.

It can be seen that the maximization of the visibility value of the measured signal V_0 can be done by the optimal choice of the Fabry–Pérot interferometer construction. A very important factor is to choose optical parameters of the material from which the mirrors are made. Furthermore, one of the critical problems of the Fabry–Pérot construction is the proper fitting of the geometrical dimension of the cavity as it influences the attenuation coefficient and, therefore, the visibility of the optical signal intensity due to the divergence of a light beam in the Fabry–Pérot cavity.

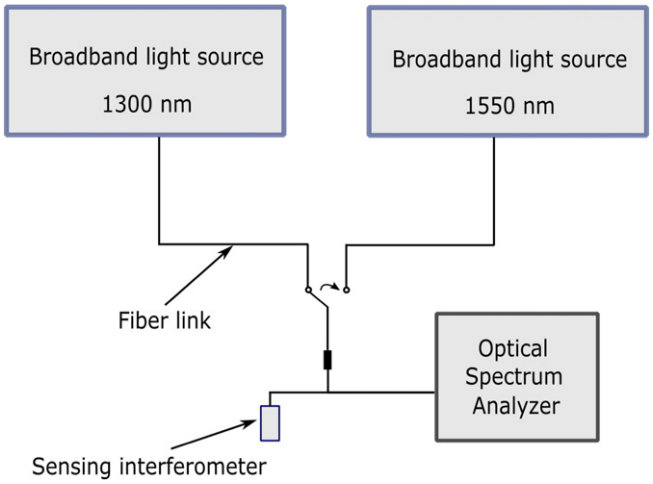

Fig. 4. The experimental set-up.

3. Materials and method

3.1. Nanocrystalline diamond film growth

Diamond films were synthetized in an MWPACVD system (SEKI Technotron AX5400S, Japan) on silicon substrates (Si-100). The use of nanodiamond DMSO/PVA base slurry with crystallites size 4–7 nm. The substrates were seeded by means of spin-coating: 60 s with 4000 rpm.

Diamond thin films were deposited using the microwave plasma assisted chemical vapor deposition (μPE CVD). The substrate temperature was approximately at 500 °C and the plasma excitation was achieved by the microwave radiation (2.45 GHz). The base pressure inside the chamber was 10^{-4} Torr and the process pressure 50 Torr. The mixture of hydrogen, methane (1%) and diborane: hydrogen mixture (for boron-doped samples — 5%, for undoped samples — 0%) filled the chamber. The doping level of boron in the gas phase was 10,000 ppm. The growth time was 60 min. Produced diamond films have thickness in the range of 200–300 nm.

3.2. Raman spectra of diamond films

The chemical composition of the thin diamond films was investigated by Raman spectroscopy, using a confocal Raman microscope. The system comprised of: an excitation source — 532 nm diode pumped solid state (DPSS) laser, a 50× magnification objective (NA = 0.75), and a 50 μm confocal aperture diode. Spectra were recorded in the range of 200–3500 cm^{-1} with measurement integration time of 100 s.

The Raman spectra of diamond films deposited on silicon substrates are shown in Fig. 2. The spectra are typical to microcrystalline diamond films, which is also in good agreement with SEM images below (Fig. 3). Strong and sharp diamond peaks were observed for 1325 cm^{-1}. The sharp peak at 520 cm^{-1} is assigned to silicon substrate.

Moreover, for the samples of doped diamond a band derived from the boron doping (481 cm^{-1} and 1231 cm^{-1}) can be observed. The latter peak is asymmetrical. This phenomenon is attributable to the Fano effect [22]. It confirms the effective doping of the diamond films by boron atoms.

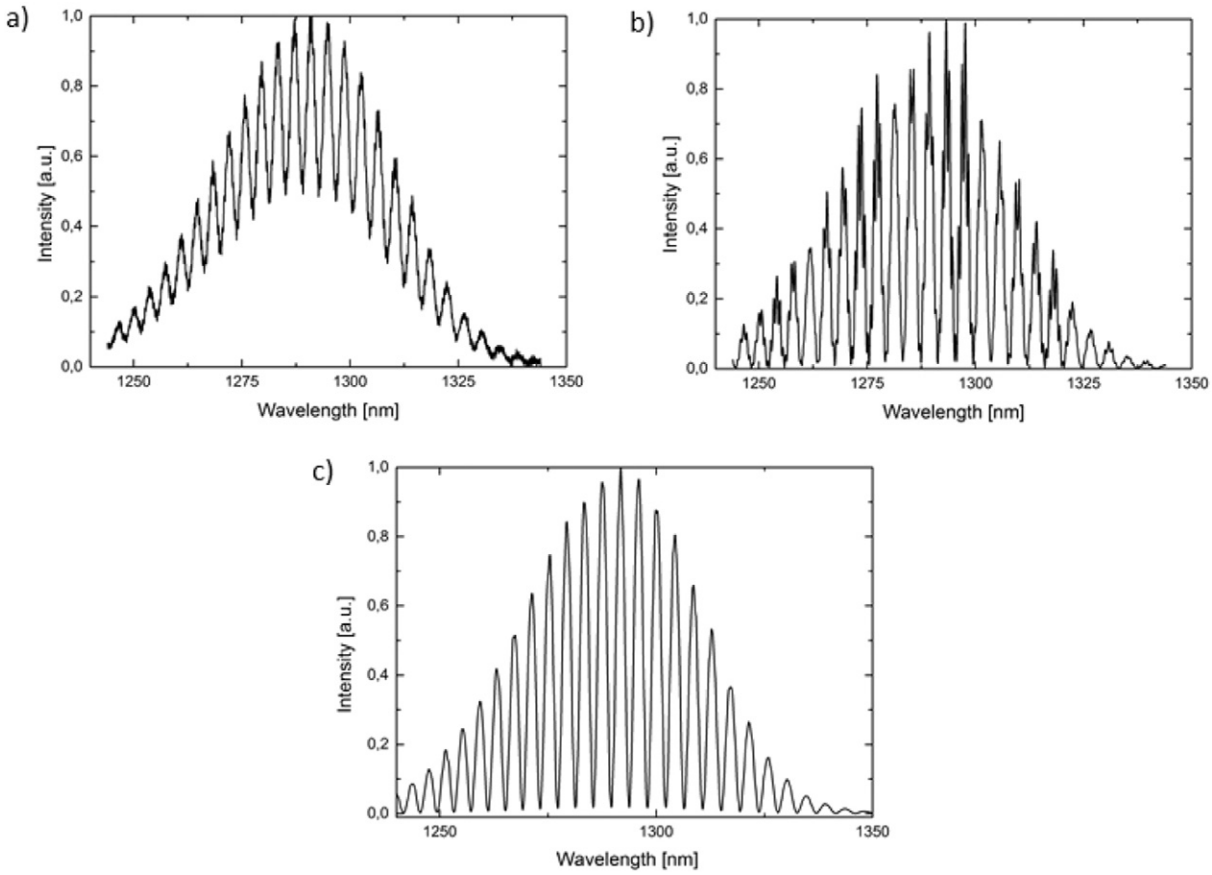

Fig. 5. The measurement signal from sensors with: a) the boron-doped diamond film, b) the undoped diamond film, c) the silver layer. During the experiment the light source with the central wavelength 1290 nm was used.

3.3. SEM images of diamond films

The scanning electron microscope with tungsten source and variable chamber pressure (VP-SEM) was used to define the surface of synthesized thin films.

Fig. 3 shows SEM micrographs of the diamond morphology on the silicon substrate. Complete coverage of the surface and the continuity of the layers can be observed. Decrease of crystallites size with the addition of boron dopant [23] can be observed for silicon substrates.

3.4. The fiber-optic Fabry–Pérot displacement sensor with thin diamonds films

In order to verify the possibility of using thin diamond films as a mirror of Fabry–Pérot displacement sensor, a few constructions of sensors were manufactured and tested. The structures consisted of diamond thin films with thickness of 200 nm grown on silicon substrate. Two kinds of diamond films were used: the undoped and boron-doped diamond films. The measurement system set-up is shown in Fig. 4.

The setup utilizes superluminescent diode with Gaussian spectral density (S1300-G-I-20: $\lambda = 1290$ nm, $\Delta\lambda_{FWHM} = 50$ nm and S-1550-G-I-20: $\lambda = 1550$ nm, $\Delta\lambda_{FWHM} = 45$ nm Superlum, Ireland) as a low coherence light source, connected to the sensor by a single-mode fiber SMF-28 and an Ando AQ6319 optical spectrum analyzer with resolution bandwidth set to 1 nm working as the detection setup. The fiber-optic Fabry–Pérot interferometer was formed by the uncoated end surface of the single-mode fiber and mirrors made from thin diamond films. This interferometer was connected to the measurement system. The response signals of the interferometer with different mirrors were recorded to choose optimal construction of the sensors to obtain the highest value of visibility of the measured signal, defined as:

$$V = \frac{I_{max} - I_{min}}{I_{max} + I_{min}} \tag{8}$$

where: I_{max} — the maximal intensity of the interference fringes, I_{min} — the minimal intensity of the interference fringes.

The measured spectra of the signal from the Fabry–Pérot interferometer in different configuration are shown in Figs. 5 and 6. In the first set-up, the source with the central wavelength of 1290 nm was used. In the second the source with the central wavelength of 1550 nm was used. For each source three types of mirrors were investigated: silver — to obtain the reference signal, the undoped and the boron-doped diamond film deposited on the silicon substrate.

Based on the measurement spectra and Eq. (8) it was possible to achieve the best value of the visibility for each sensor configuration.

According to data in Table 1, it can be observed that the use of undoped thin films deposited on silicon substrate, as reflective surfaces, allows achieving even higher value of visibility as when the silver mirror is used. The value of the visibility of the measured signal when undoped diamond films deposited on silicon substrate are used is smaller, yet still acceptable and interesting for sensing applications. Boron doping has the influence on surface morphology and chemical structure as well optical properties: refractive index, extinction coefficient and absorption coefficient. Boron concentration has the effect of reduction of crystallite size.

4. Results and discussion

In the elaborated sensor, the difference between interfering beams reflected from mirrors of the Fabry–Pérot cavity depends on the

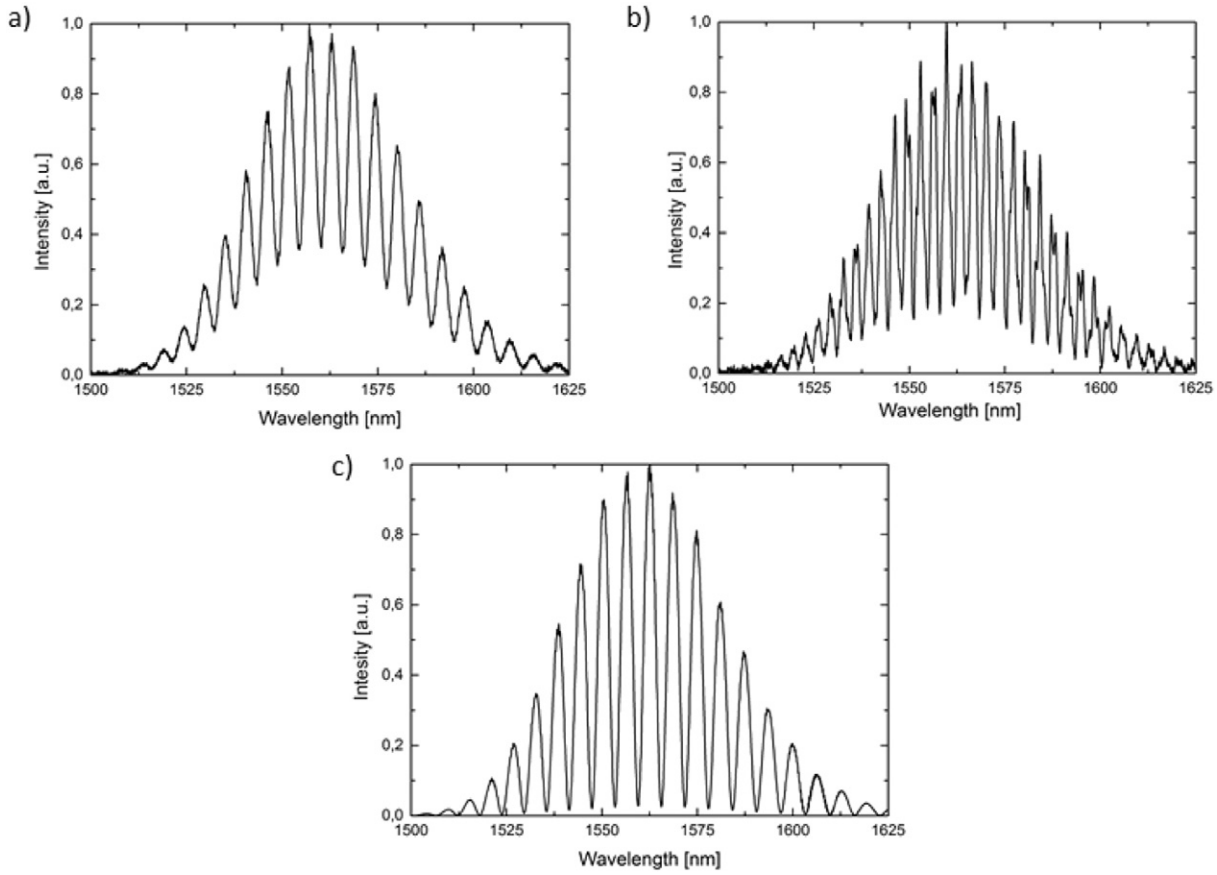

Fig. 6. The measurement signal from sensors with: a) the boron-doped diamond film, b) the undoped diamond film, c) the silver layer. During the experiment the light source with the central wavelength 1550 nm was used.

distance between them. Any change of the phase difference between interfering beams modifies the spectrum of the reflected signal $I(\nu)$ according to the following equation [21,24]:

$$I(\nu) = S(\nu)R(\nu) \tag{9}$$

where: $S(\nu)$ — the spectral distribution of the light source; $R(\nu)$ — reflectivity of the Fabry–Pérot sensing interferometer.

The measured signal obtained from sensors in different configurations is shown in Figs. 7, 8, and 9. Representative spectra measured for different displacements are presented.

The visibility of the measured signal presented in Figs. 7, 8, and 9 is good enough to confirm the validity of the designed approach. Comparing the spectra from each figure a) part measured for the distance 300 μm with part b) measured for the distance 450 μm it is possible to note the difference between the distances between maximums in the measured signal spectra caused by the change in the length of the interferometer cavity.

The analysis of the obtained spectra was based on the calculation of spectral separation for each measured displacement, ranging from 50 to 600 nm. The dependence of the displacement on the spectral separation is plotted in Fig. 10.

Table 1
The visibility of the measured signal in the Fabry–Pérot interferometer.

Mirror material	The central wavelength of light source: 1290 nm	The central wavelength of light source: 1550 nm
Silver	94.3%	94.4%
Undoped diamond film on silicon substrate	95.6%	66.9%
Boron-doped diamond film on silicon substrate	33.4%	45.8%

It can be noted that presented results are well characterized by nonlinear dependence of displacement on the spectral separation. The analysis of the regression of obtained results indicates that it is possible to estimate a trend line of results. Equations describing trend lines in the form of exponential curves are presented in Fig. 10.

In order to assess whether the regression model explains the experimental results, coefficient of determination R^2 should be calculated. It is described by following expression:

$$R^2 = \frac{\sum_{i=1}^{N}(x_p-\mu)^2}{\sum_{i=1}^{N}(\bar{x}-\mu)^2},$$

where x_p is the value expected by the regression model, μ is the mean, x is measured value of spectral separation.

Calculated coefficients of determination were also shown in Fig. 10 and are ranging from 0.9565 to 0.9967. This indicates that regression model fits almost perfectly to presented results.

Results were compared with results from silver mirror, commonly used as a reflective surface in the Fabry–Pérot interferometers. Characteristics of interferometers using different layers are shown in Fig. 11.

As can be seen in Fig. 11a, in case of measurements with a source with the central wavelength $\lambda = 1290$ nm, undoped and boron-doped diamond layers provide the similar sensitivity of a sensor as sensor with silver mirror.

In case of measurements with a source with the central wavelength $\lambda = 1550$ nm, boron-doped diamond is the layer that has similar characteristic of the spectral separation of the measured signal vs. the displacement as that for sensor with silver mirror. The characteristic of

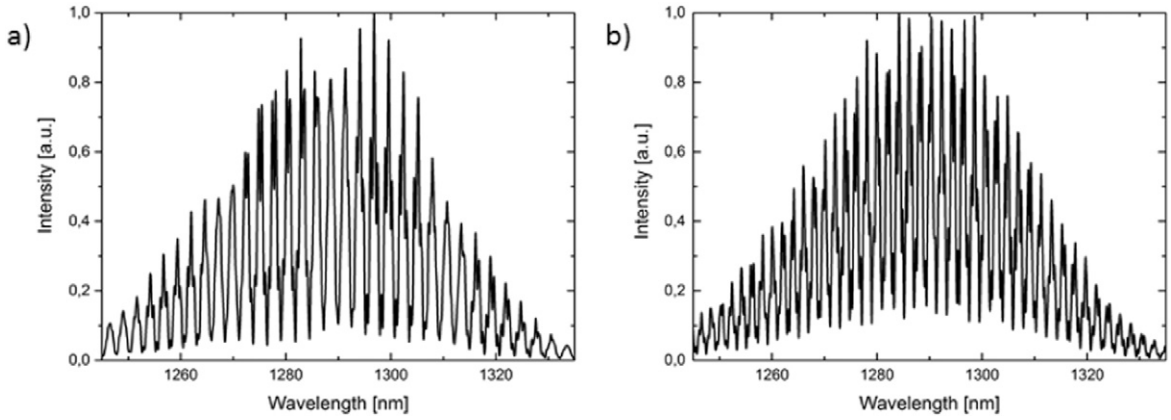

Fig. 7. The measurement signal with the central wavelength 1290 nm and the undoped diamond film. The length of Fabry–Pérot cavity is: a) 300 μm, b) 400 μm. The undoped diamond film was used.

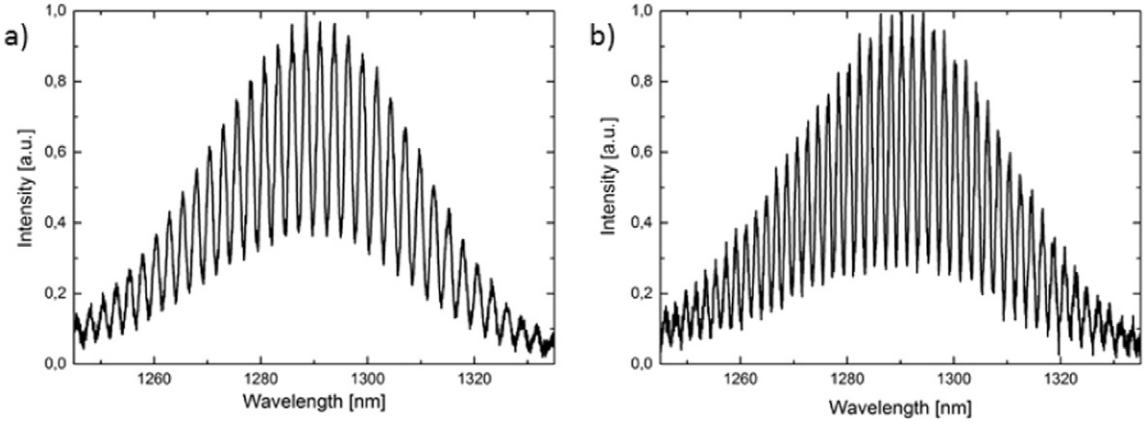

Fig. 8. The measurement signal with the central wavelength 1290 nm and the boron doped diamond film. The length of Fabry–Pérot cavity is: a) 300 μm, b) 400 μm.

undoped diamond has no such slope as silver mirror, but it provides sufficient sensitivity so it can be utilized in reflective layers. The boron-doped diamond characteristic deviates slightly from silver mirror, but considering the benefits of using this material in the reflective layer (e.g., resistance to mechanical damage and harmful chemical conditions), the result is satisfactory for sensor applications.

The sensor characterization was made in the distance range extending from 50 to 600 μm with resolution equal to 10 μm. The output signal was analyzed by measurement of the change of the spectral separation between the maxima in spectral pattern.

Bearing in mind the obtained results, it can be concluded that the examination of the diamond film, as the mirror in the fiber-optic Fabry–Pérot interferometric displacement sensor, proves its capability of the distance measurement along with satisfactory metrological parameters.

5. Conclusions

This article describes the use of thin diamond film as mirror of Fabry–Pérot displacement sensor. Diamond thin films were deposited using the microwave plasma assisted chemical vapor deposition on

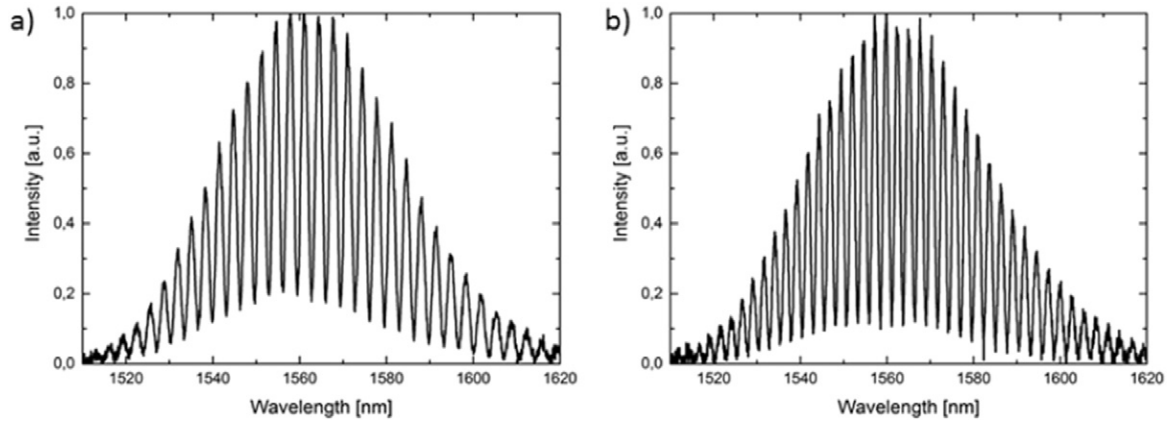

Fig. 9. The measurement signal with the central wavelength 1550 nm and the boron doped diamond film. The length of Fabry–Pérot cavity is: a) 350 μm, b) 450 μm.

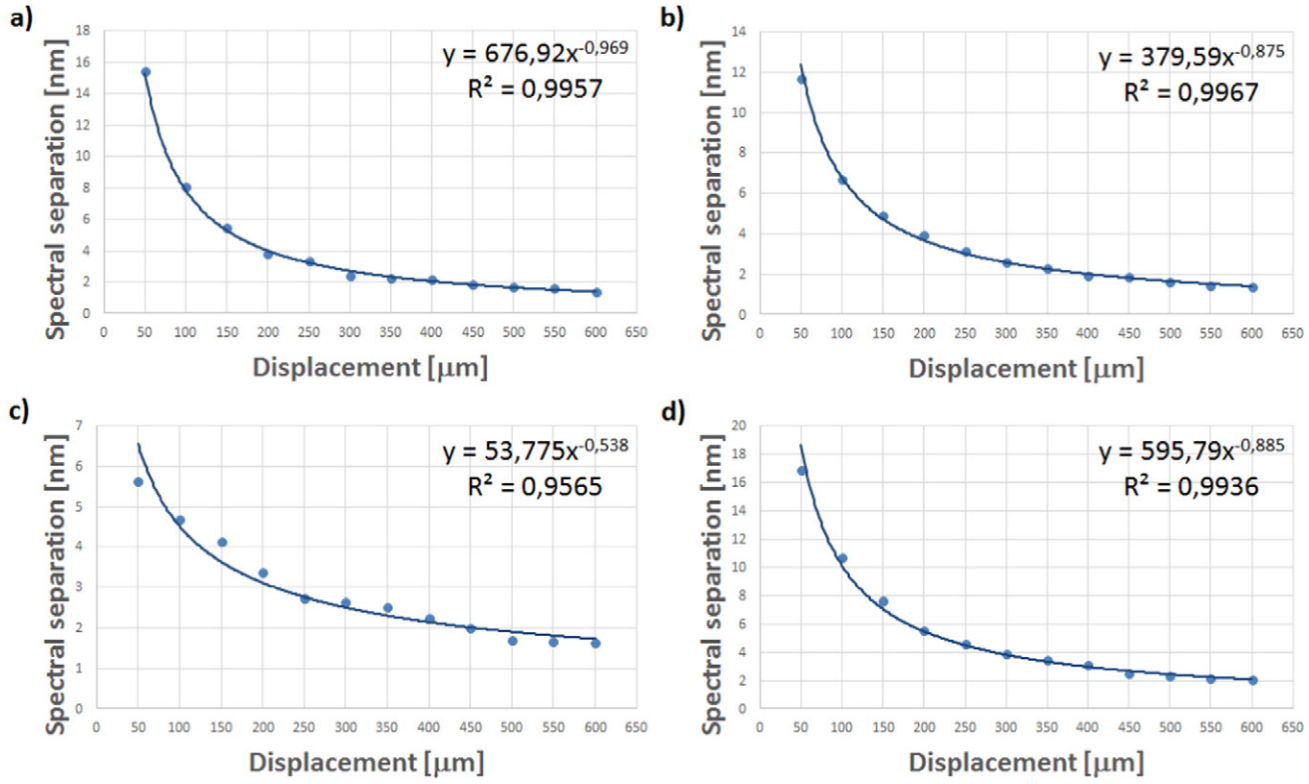

Fig. 10. The spectral separation of the measured signal vs. the displacement for: a) the undoped diamond and b) the boron-doped diamond film, and source with the central wavelength λ = 1290 nm; c) the undoped diamond and d) the boron-doped diamond, and source with the central wavelength λ = 1550 nm.

silicon substrates. The dependency of the fiber-optic interferometer signal on distance changes in the low-coherence measurement set-up with signal processing in spectral domain was examined. An asymmetric configuration of the Fabry–Pérot interferometer working in reflective mode was implemented. Such an interferometer was selected due to its advantages that include the relatively simple configuration, potentially low manufacturing cost and high resolution of measurement. Moreover, owing to its small size, it makes it viable to take high spatial resolution measurements.

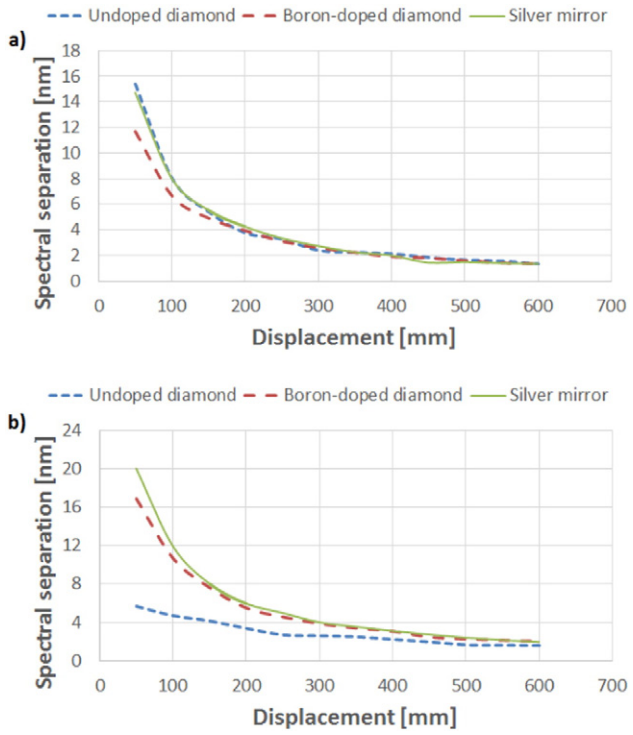

Fig. 11. The comparison of characteristics of interferometers using different layers: a) for a source with the central wavelength λ = 1290 nm; b) for a source with the central wavelength λ = 1550 nm.

The examination of the sensors' metrological parameters proves its capability to measure the distance with good measurement parameters. The illustrated preliminary results provide the base for constructing biophotonic sensors ready for functional applications.

With a possible application of a fiber-optic low-coherence Fabry–Pérot interferometer as a biosensor, the reflective surface should be biocompatible with the measured sample (e.g., bodily fluids) and provide great chemical stability.

Prime novelty statement

Fabry–Pérot interferometer in fiber-optic configuration is widely used for sensing application. It can be constructed using various materials as reflective elements, e.g., silver mirrors, zinc oxide layers, and photonic fibers [1–5]. In this article we describe the first application of thin diamond films in a low-coherence fiber-optic Fabry–Pérot sensor. Furthermore, developed sensor was successfully used for displacement measurements.

1. Wei, T; Han, YK; Tsai, HL; Xiao, H; "Miniaturized fiber inline Fabry–Perot interferometer fabricated with a femtosecond laser," Optics Letters Vol. 33, Issue 6, pp. 536–538 (2008).

2. Choi, HY; Park, KS; Park, SJ; Paek, UC; Lee, BH; Choi, ES; "Miniature fiber-optic high temperature sensor based on a hybrid structured Fabry–Perot interferometer," Optics Letters Vol. 33, Issue 21, pp. 2455–2457 (2008).

3. Rao, YJ; "Recent progress in fiber-optic extrinsic Fabry–Perot interferometric sensors," Optical Fiber Technology Vol. 12, Issue 3, pp. 227–237 (2006).

4. Murphy, KA; Gunther, MF; Vengsarkar, AM; Claus, RO; "Quadrature phase-shifted, extrinsic Fabry–Perot optical fiber sensors," Optics Letters Vol. 16, Issue 4, pp. 273–275 (1991).

5. Fan, XD; White, IM; Shopova, SI; Zhu, HY; Suter, JD; Sun., YZ; "Sensitive optical biosensors for unlabeled targets: A review," Analytica Chimica Acta Vol. 620, Issue 1–2, pp. 8–26 (2008).

Acknowledgments

This study was partially supported by the National Science Centre, Poland grant no. 2011/03/D/ST7/03540 and DS Funds of the Faculty of Electronics, Telecommunications and Informatics, Gdańsk University of Technology.

References

[1] M. Jędrzejewska-Szczerska, P. Wierzba, A.A. Chaaya, M. Bechelany, P. Miele, R. Viter, A. Mazikowski, K. Karpienko, M.S. Wróbel, ALD thin ZnO layer as an active medium in a fiber-optic Fabry–Perot interferometer, Sensors Actuators A Phys. 221 (2015) 88–94.

[2] K. Karpienko, M.S. Wróbel, M. Jędrzejewska-Szczerska, Determination of refractive index dispersion using fiber-optic low-coherence Fabry–Perot interferometer: implementation and validation, Opt. Eng. 53 (7) (2014).

[3] D. Duraibabu, K. Kalli, G. Leen, G. Dooly, E. Lewis, J. Kelly, M. Munroe, Recent improvement of medical optical fibre pressure and temperature sensors, Biosensors 5 (3) (2015) 432–449.

[4] Md.R. Islam, M.M. Ali, M. Lai, K. Lim, H. Ahmad, Chronology of Fabry–Perot interferometer fiber-optic sensors and their applications: a review, Sensors 14 (4) (2014) 7451–7488.

[5] Y. Rao, M. Deng, D. Duan, T. Zhu, In-line fiber Fabry–Perot refractive-index tip sensor based on endlessly photonic crystal fiber, Sensors Actuators A Phys. 148 (1) (2008) 33–38.

[6] J. Eom, C. Park, B.H. Lee, J. Lee, I. Kwon, E. Chung, Fiber optic Fabry–Perot pressure sensor based on lensed fiber and polymeric diaphragm, Sensors Actuators A Phys. 225 (2015) 25–32.

[7] W.J. Wang, R.M. Lin, D.G. Guo, T.T. Sun, Development of a novel Fabry–Perot pressure microsensor, Sensors Actuators A Phys. 116 (1) (2004) 59–65.

[8] C. Lin, F. Tseng, A micro Fabry–Perot sensor for nano-lateral displacement sensing with enhanced sensitivity and pressure resistance, Sensors Actuators A Phys. 114 (2) (2004) 163–170.

[9] M. Jiang, E. Gerhard, A simple strain sensor using a thin film as a low-finesse fiber-optic Fabry–Perot interferometer, Sensors Actuators A Phys. 88 (1) (2001) 41–46.

[10] M. Jędrzejewska-Szczerska, Response of a new low-coherence Fabry–Perot sensor to hematocrit levels in human blood, Sensors 14 (4) (2014) 6965–6976.

[11] M. Jędrzejewska-Szczerska, Measurement of complex refractive index of human blood by low-coherence interferometry, Eur. Phys. J. Spec. Top. 222 (9) (2013) 2367–2372.

[12] M. Jędrzejewska-Szczerska, M. Gnyba, Optical investigation of hematocrit level in human blood, Acta Phys. Pol. A 120 (4) (2011) 642–647.

[13] K.T.V. Grattan, B.T. Meggitt, Optical Fiber Sensor Technology, Kluwer Academic Publisher, Boston, 2000.

[14] B. Culshaw, J. Dakin, Optical Fiber Sensors: Systems and Applications, Norwood, Artech House, 1989.

[15] T. Liu, D. Brooks, A. Martin, R. Badcocko, G. Fernando, Design, fabrication, and evaluation of an optical fiber sensor for tensile and compressive strain measurements via the use of white light interferomerty, Proc. SPIE 2718 (1996) 408–416.

[16] M. Sobaszek, Ł. Skowroński, R. Bogdanowicz, K. Siuzdak, A. Cirocka, P. Zięba, M. Gnyba, M. Naparty, Ł. Gołuński, P. Płotka, Optical and electrical properties of ultrathin transparent nanocrystalline boron-doped diamond electrodes, Opt. Mater. 42 (2015) 24–34.

[17] A.V. Sukhadolau, E.V. Ivakin, V.G. Ralchenko, A.V. Khomich, A.V. Vlasov, A.F. Popovic, Thermal conductivity of CVD diamond at elevated temperatures, Diam. Relat. Mater. 14 (2005) 589–593.

[18] X. Checoury, D. Neel, P. Boucaud, C. Gesset, H. Girard, S. Saada, P. Bergonzo, Nanocrystalline diamond photonics platform with high quality factor photonic crystal cavities, Appl. Phys. Lett. 101 (2012) 171115.

[19] J. Stotter, S. Haymond, J.K. Zak, Y. Show, Z. Cvackova, G.M. Swain, Optically transparent diamond electrodes for UV–vis and IR spectroelectrochemistry, Interface 12 (2003) 33.

[20] M. Amaral, A.G. Dias, P.S. Gomes, M.A. Lopes, R.F. Silva, J.D. Santos, M.H. Fernandes, Nanocrystalline diamond: on vitro biocompatibility assessment by MG63 and human bone marrow cells cultures, J. Biomed. Mater. Res. 87 (1) (2008) 91–99.

[21] P. Hariharan, Optical Interferometry, second ed. Academic Press Elsevier Science, San Diego, 2003.

[22] A. Zimmer, O.A. Williams, K. Haenen, H. Terryn, Optical properties of heavily boron-doped nanocrystalline diamond films studied by spectroscopic ellipsometry, Appl. Phys. Lett. 93 (2008) 131910.

[23] X.Z. Liao, R.J. Zhang, C.S. Lee, S.T. Lee, Y.W. Lam, The influence of boron doping on the structure and characteristics of diamond thin films, Diam. Relat. Mater. 6 (1997) 521–525.

[24] S. Egorov, A. Mamaev, I. Likhachiev, High reliable, self-calibrated signal processing method for interferometric fiber-optic sensors, Proc. SPIE 2594 (1996) 193–197.